

## Gogny-HFB+QRPA dipole strength function and its application to radiative nucleon capture cross section

S. Goriely,<sup>1</sup> S. Hilaire,<sup>2</sup> S. Péru,<sup>2</sup> and K. Sieja<sup>3</sup>

<sup>1</sup>*Institut d'Astronomie et d'Astrophysique, Université Libre de Bruxelles, CP-226, 1050 Brussels, Belgium*

<sup>2</sup>*CEA, DAM, DIF, F-91297 Arpaçon, France*

<sup>3</sup>*Université de Strasbourg, IPHC, 23 rue du Loess 67037 Strasbourg, France CNRS, UMR7178, 67037 Strasbourg, France*



(Received 29 March 2018; published 30 July 2018)

Valuable theoretical predictions of nuclear dipole excitations in the whole nuclear chart are of great interest for different applications, including in particular nuclear astrophysics. Here we extend our large-scale calculations of the  $E1$  and  $M1$  absorption  $\gamma$ -ray strength function obtained in the framework of the axially symmetric deformed quasiparticle random-phase approximation (QRPA) based on the finite-range DIM Gogny force to the deexcitation strength function. To do so, shell-model calculations of the deexcitation dipole strength function are performed and their limit at low  $\gamma$  energies used to complement phenomenologically the QRPA calculations. We compare our final prediction of the  $E1$  and  $M1$  strength with available experimental data at low energies and show that a fairly good agreement is obtained. Predictions of the dipole strength function for spherical and deformed nuclei within the valley of  $\beta$  stability as well as in the neutron-rich region are discussed and compared with traditional Lorentzian-type prescriptions. Its impact on the total radiative width as well as radiative neutron and proton capture cross sections is studied.

DOI: [10.1103/PhysRevC.98.014327](https://doi.org/10.1103/PhysRevC.98.014327)

### I. INTRODUCTION

Radiative neutron capture cross sections play a key role in almost all nuclear applications. Despite a huge effort to measure such radiative neutron capture cross sections, theoretical predictions are required to fill the gaps, both for nuclei for which measurements are not feasible at the present time, in particular for unstable targets, and for energies that cannot be reached in the laboratory. Some applications, such as nuclear astrophysics, also require the determination of radiative neutron capture cross sections for a large number of exotic neutron-rich nuclei [1]. In this case, large-scale calculations need to be performed on the basis of sound and accurate models to ensure a reliable extrapolation far away from the experimentally known region.

The neutron capture rates are commonly evaluated within the framework of the statistical model of Hauser-Feshbach, although the direct capture contribution plays an important role for very exotic nuclei [2]. The fundamental assumption of the Hauser-Feshbach model is that the capture goes through the intermediary formation of a compound nucleus in thermodynamic equilibrium. In this approach, the  $(n, \gamma)$  cross section strongly depends on the electromagnetic interaction, i.e., the photon deexcitation probability. In turn, it is well known that the photon strength function is dominated by the dipole contribution. The various multipolarities of the  $\gamma$ -ray strength function are traditionally modeled by the phenomenological Lorentzian approximation or some of its energy-dependent variants [3].

The reliability of the  $\gamma$ -ray strength predictions can, however, be greatly improved by the use of microscopic or semimicroscopic models. Such an effort can be found in Refs. [4–8]

where a complete set of  $E1$  and  $M1$   $\gamma$ -ray strength functions was derived from mean-field-plus-quasiparticle random-phase approximation (QRPA) calculations. When compared with experimental data and considered for practical applications, all mean-field-plus-QRPA calculations need, however, some phenomenological corrections. These include a broadening of the QRPA strength to take the neglected damping of collective motions into account as well as a shift of the strength to lower energies due to the contribution beyond the one-particle–one-hole excitations and the interaction between the single-particle and low-lying collective phonon degrees of freedom [9–16]. In addition, most of the mean-field-plus-QRPA calculations assume spherical symmetries, so that phenomenological corrections need to be included in a way or another in order to properly describe the splitting of the giant dipole resonance in deformed nuclei. State-of-the-art calculations including effects beyond the one-particle–one-hole excitations and phonon coupling are now available [9–16] but they remain computer-wise intractable for large-scale applications.

Recently, axially symmetric-deformed QRPA calculations based on Hartree-Fock-Bogoliubov (HFB) calculations using the finite-range Gogny interaction have been shown to provide rather satisfactory predictions of the  $E1$  [7] and  $M1$  strengths [8]. However, such QRPA calculations only describe the photoabsorption and it is now well accepted that the deexcitation strength function may differ from the photoabsorption one, especially at low photon energies [3, 17]. In particular, a non-zero limit of the dipole strength has been observed experimentally [18, 19] and confirmed by shell model (SM) calculations [20–25].

In the present paper, we extend our previous HFB+QRPA study of the  $E1$  and  $M1$  photoabsorption strength [7, 8] to

the deexcitation strength including a low-energy limit inspired from SM calculation and adjusted on existing low-energy data. The paper is organized as follows. In Sec. II, the  $E1$  and  $M1$  HFB+QRPA dipole photoabsorption strength functions are rapidly described together with the way corrections beyond QRPA are included phenomenologically. The deexcitation dipole strength function is discussed in Sec. III and low-energy contributions introduced to take into account the predictions of the SM and available experimental data. In Sec. IV, we compare measured average radiative width obtained with our DIM+QRPA strength and with Lorentzian-type models. Finally, the impact of the newly calculated  $\gamma$ -ray strength functions on the Hauser-Feshbach estimate of the radiative neutron and proton capture cross sections is studied and compared with results obtained with more traditional Lorentzian-type prescriptions in Sec. V. Conclusions are drawn in Sec. VI.

## II. THE DIM+QRPA DIPOLE STRENGTH

The QRPA formalism based on axially symmetric-deformed HFB equations solved in a finite harmonic oscillator basis in cylindrical coordinates has been described in detail in Refs. [7,8,26–29]. In the present study, the DIM Gogny force [30] is used. Previous studies [7] have shown that the experimental peak energy of the giant dipole resonance (GDR) (lying typically around 13–16 MeV [31]) is systematically overestimated by our DIM+QRPA calculations by typically 2.5 MeV; this is a general rule for spherical as well as deformed nuclei. Similarly, a study of the QRPA low-energy vibrational states shows that the first experimental energies [32] are overestimated by typically 500 keV, as shown in Fig. 1. For this reason, the effects beyond the one-particle–one-hole QRPA can be empirically included by considering an energy shift that increases with energy. In comparison with our previous study of the  $E1$  QRPA strength [7], we now adopt a simpler treatment of the renormalization procedure to reproduce both the experimental GDR properties and low-energy vibrational states. More specifically, for the  $E1$  and  $M1$  QRPA strength, we now apply an energy shift of  $\Delta = 0.5$  MeV for  $\varepsilon_\gamma \leq 0.5$  MeV,  $\Delta = 2.5$  MeV for  $\varepsilon_\gamma = 18$  MeV, and  $\Delta = 5$  MeV for  $\varepsilon_\gamma \geq 21$  MeV. For energies in the  $0.5 \leq \varepsilon_\gamma \leq 21$  MeV range, the energy shift  $\Delta$  is interpolated linearly between the anchor values at 0.5, 18, and 21 MeV.

Similarly, an empirical damping of the collective motions is introduced in the QRPA strength by folding each  $E1$  strength by a standard Lorentzian (SLO) function of width  $\Gamma$  that has been adjusted on photoabsorption data and is assumed to be dependent on the atomic mass  $A$  only. We adopt the final expression  $\Gamma$  (MeV) =  $7 - A/45$  for  $A \leq 200$  and 2.5 MeV otherwise. For the  $M1$  strength, a constant value of  $\Gamma = 0.5$  MeV is adopted [8].

With such a systematic renormalization of the HFB+QRPA calculations, experimental strength functions based on photoabsorption measurements (see also Fig. 7 below) or nuclear resonance fluorescence can be rather well described, as already shown in Refs. [7,8]. In particular, we compare in Figs. 2 and 3 the strength functions extracted from photoabsorption data [33] with the DIM+QRPA calculations for some 60

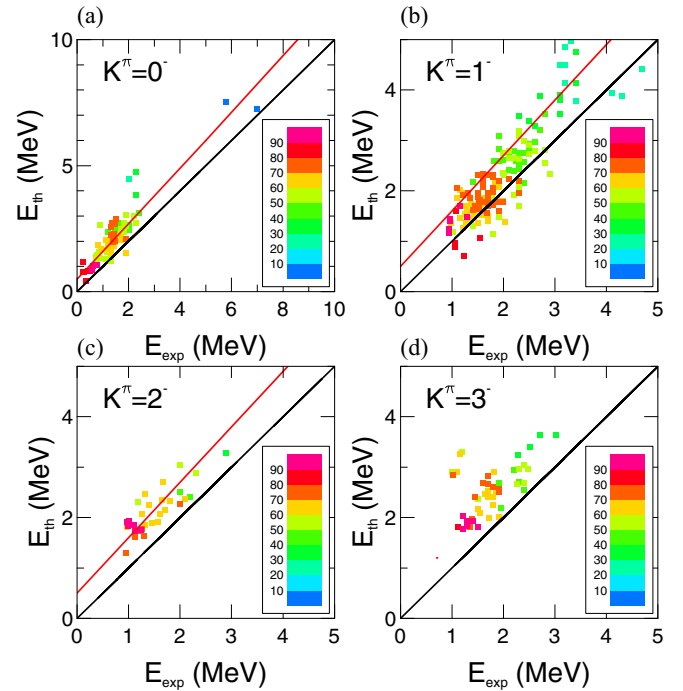


FIG. 1. Experimental–theoretical comparison of the energy of the low-energy vibrational states (a)  $K^\pi = 0^-$ , (b)  $K^\pi = 1^-$ , (c)  $K^\pi = 2^-$ , and (d)  $K^\pi = 3^-$ . The red curve corresponds to the energy shift applied to the HFB+QRPA strength. The color code refers to the atomic mass range of the nuclei.

nuclei lying between  $^{72}\text{Ge}$  and  $^{198}\text{Pt}$ . Strengths for spherical as well as deformed nuclei are rather satisfactorily described in the 10- to 20-MeV photon energy range in terms of GDR centroid energy, width of the resonance, and overall amplitude of the strength. For some strongly deformed prolate nuclei, like  $^{176}\text{Hf}$ , the ratio of the two GDR peaks is found to be inverted with respect to photoabsorption data. This inversion could originate either from an oblate, instead of a prolate, deformation like in  $^{194}\text{Pt}$  or a smaller quadrupole deformation like the one characterizing  $^{190}\text{Os}$ . However, such an inversion is mainly a consequence of the folding procedure which assumes an energy-independent width applied similarly to both the  $K^\pi = 0^-$  and  $1^-$  components.

## III. $E1$ AND $M1$ DEEXCITATION STRENGTH FUNCTION

When considering the deexcitation strength function, deviations from the photoabsorption strength can be expected, especially for  $\gamma$ -ray energies approaching the zero limit. While studies in the framework of the temperature-dependent linear response theory for superfluid Fermi liquids have been performed for some decades [34], little microscopic calculations of the  $E1$  and  $M1$  deexcitation strength function are practically available today, especially for their low-energy limit [35,36]. Recently, new calculations within the SM framework have been performed for both the  $E1$  and  $M1$  modes. In particular, it was found [22] that the  $E1$  remains constant at energies  $\varepsilon_\gamma \lesssim 5$  MeV. In addition, available SM calculations [20–25] all

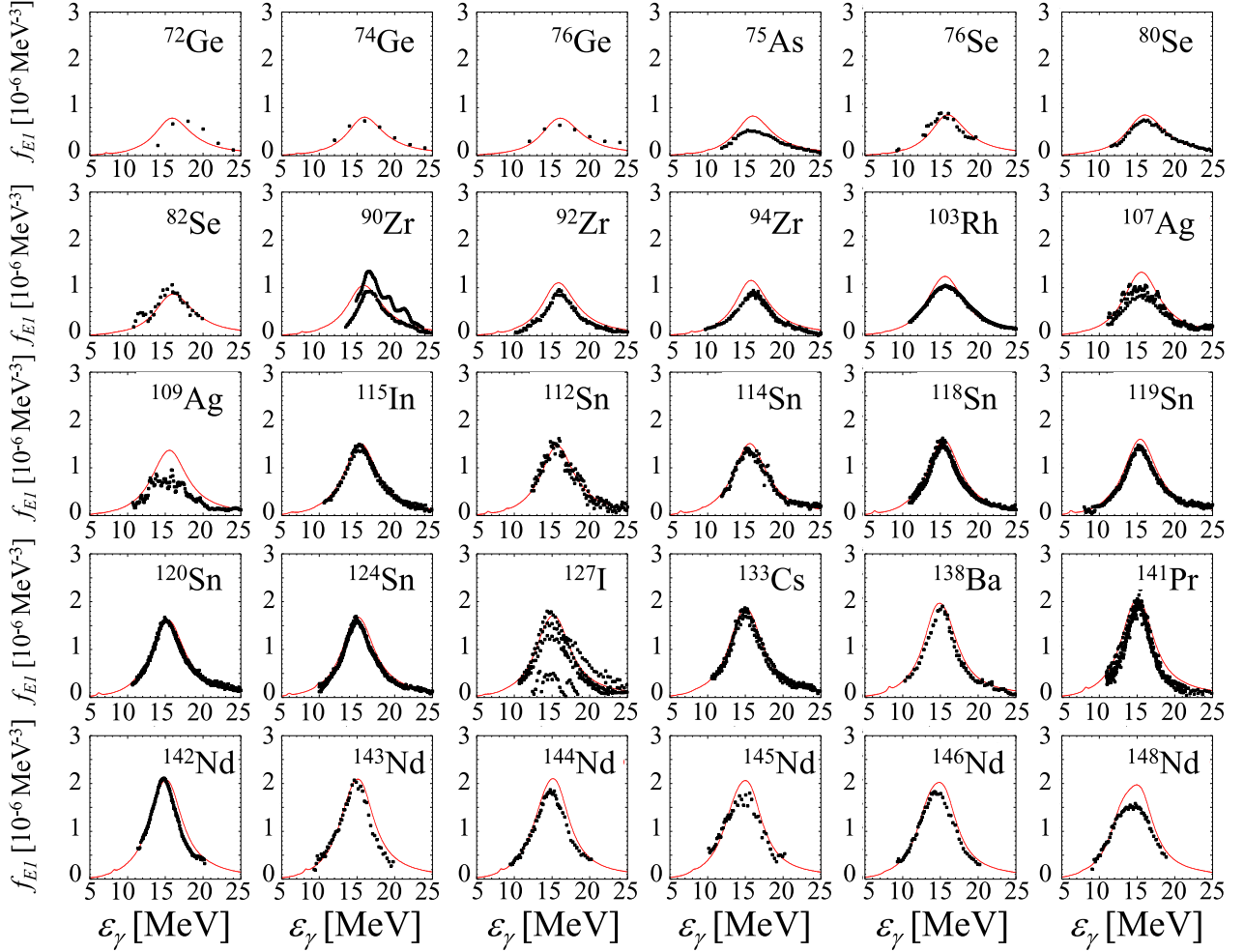


FIG. 2. Comparison of the experimental GDR strength [33] (black squares) with the DIM+QRPA predictions (red lines) for 30 nuclei between  $^{72}\text{Ge}$  and  $^{148}\text{Nd}$ .

predict an exponential increase of the  $M1$  deexcitation strength function at decreasing energies approaching zero. The upbend of the strength function observed experimentally [18,19] has therefore been assumed to be of the  $M1$  nature, though no experimental evidence exists for the moment. The low-energy limits obtained by SM were found to be relatively insensitive to the excitation energy  $U$  of the initial decaying state for the  $M1$  strength (see, e.g., Ref. [23]) and for the  $E1$  strength, as shown in Fig. 4.<sup>1</sup> The deexcitation strength function can therefore be taken from the QRPA calculation (Sec. II) provided additional contributions at low energies inspired from SM predictions are included.

The final  $E1$  and  $M1$  strengths, including the low-energy contributions and hereafter denoted as DIM+QRPA+0lim,

<sup>1</sup>Note that throughout this paper we use the definition  $f_{X1}(E_i, E_\gamma, J, \pi) = 16\pi/9(\hbar c)^3 \langle B(X1; E_i, E_\gamma, J, \pi) \rangle \rho(E_i, J, \pi)$  (where  $X = M$  or  $E$ ) to extract the radiative strength from the SM results. This expression leads to lower values in comparison with previous studies [20–25], which used to estimate the strength on the basis of the total level densities  $\rho(E_i)$ .

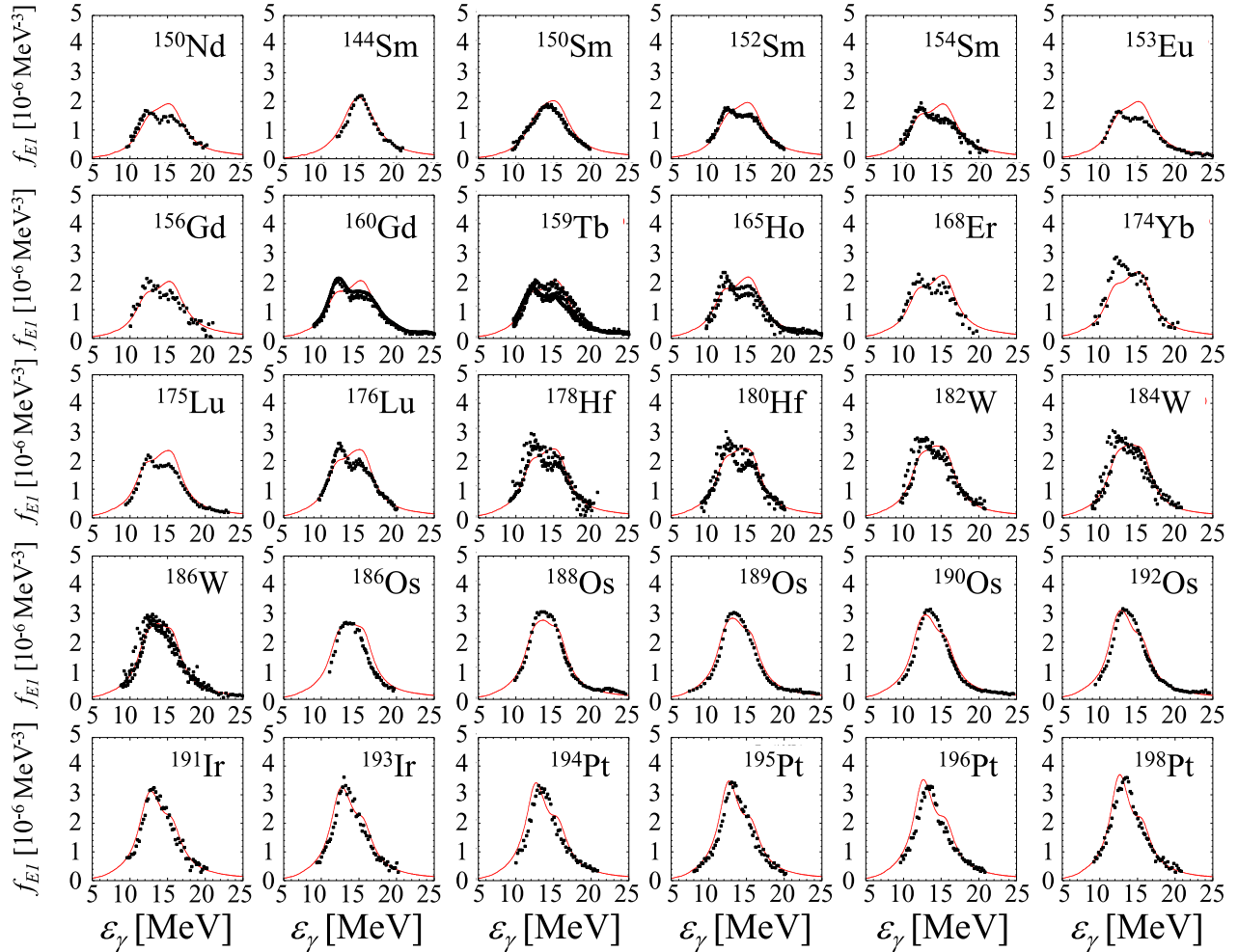
can be expressed as

$$\overleftarrow{f}_{E1}(\varepsilon_\gamma) = f_{E1}^{\text{QRPA}}(\varepsilon_\gamma) + f_0 U / [1 + e^{(\varepsilon_\gamma - \varepsilon_0)}], \quad (1)$$

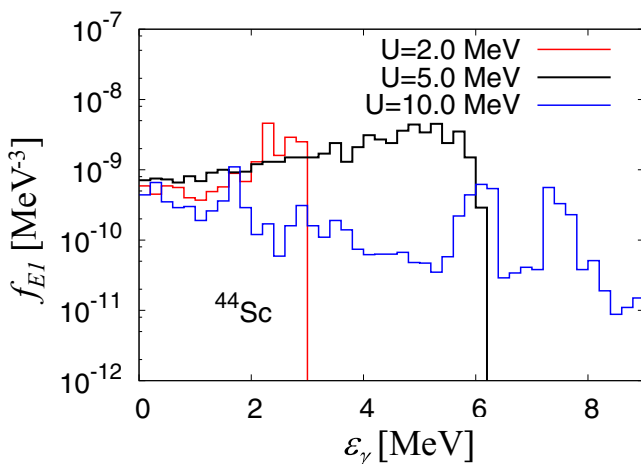
$$\overleftarrow{f}_{M1}(\varepsilon_\gamma) = f_{M1}^{\text{QRPA}}(\varepsilon_\gamma) + C e^{-\eta \varepsilon_\gamma}, \quad (2)$$

where  $f_{X1}^{\text{QRPA}}$  is the DIM+QRPA dipole strength at the photon energy  $\varepsilon_\gamma$ ,  $U$  (in MeV) is the excitation energy of the initial deexciting state and  $f_0$ ,  $\varepsilon_0$ ,  $C$ , and  $\eta$  are free parameters that can be adjusted on SM results and available low-energy experimental data such as those obtained with the Oslo method [18,19,37] or the average radiative widths [3] (see below). The low-energy limit of the  $M1$  strength is assumed here to be independent of the deformation, although following SM studies [23–25], it was found that, for deformed nuclei, the  $M1$  upbend is less pronounced, part of the strength being transferred into the scissors mode region.

The impact of the low-energy limit applied to the DIM+QRPA strength is illustrated in Fig. 5 for the  $E1$  channel in  $^{44}\text{Ti}$  where the values of  $f_0 = 10^{-10} \text{ MeV}^{-4}$  and  $\varepsilon_0 = 3 \text{ MeV}$  are considered for the low-energy strength [Eq. (1)]. Larger values around  $f_0 = 5 \times 10^{-10} \text{ MeV}^{-4}$  and  $\varepsilon_0 = 5 \text{ MeV}$

FIG. 3. Same as in Fig. 2 for 30 nuclei between  $^{150}\text{Nd}$  and  $^{198}\text{Pt}$ .

are found to be in closer agreement with the zero energy limit empirically determined within the generalized Lorentzian (GLO) approach [17].

FIG. 4. Illustration for  $^{44}\text{Sc}$  of the low-energy  $E1$  strength function predicted by the SM for three different initial excitation energies  $U$ .

For the  $M1$  strength, we compare in Fig. 6 the  $^{134}\text{Xe}$  and  $^{136}\text{Ba}$  SM predictions with those obtained with the DIM+QRPA+0lim [Eq. (2)] corresponding to the parameters  $C = 10^{-8} \text{ MeV}^{-3}$  and  $\eta = 0.8 \text{ MeV}^{-1}$ . To account for different magnitudes and slopes of the  $M1$  strengths at low energies predicted in available SM studies, Refs. [20–25], we consider in the present paper two sets of parameters leading, in a first approximation, to lower and upper limits of the low-energy contribution. These correspond to the following parameters:

- (i) lower limit (DIM + QRPA + 0lim<sup>-</sup>):  $f_0 = 10^{-10} \text{ MeV}^{-4}$ ,  $\varepsilon_0 = 3 \text{ MeV}$ ,  $C = 10^{-8} \text{ MeV}^{-3}$ ,  $\eta = 0.8 \text{ MeV}^{-1}$ .
- (ii) upper limit (DIM + QRPA + 0lim<sup>+</sup>):  $f_0 = 5 \times 10^{-10} \text{ MeV}^{-4}$ ,  $\varepsilon_0 = 5 \text{ MeV}$ ,  $C = 3 \times 10^{-8} \text{ MeV}^{-3}$ ,  $\eta = 0.8 \text{ MeV}^{-1}$ .

The total  $E1 + M1$  dipole strength obtained with Eqs. (1) and (2) is compared with experimental data extracted from photoabsorption measurements and the Oslo method in Fig. 7 for a sample of 4 nuclei and in Fig. 8 for 30 nuclei for which Oslo data are available. Note that the dipole strength data extracted from the Oslo method only include experimental systematic uncertainties and not model-dependent statistical

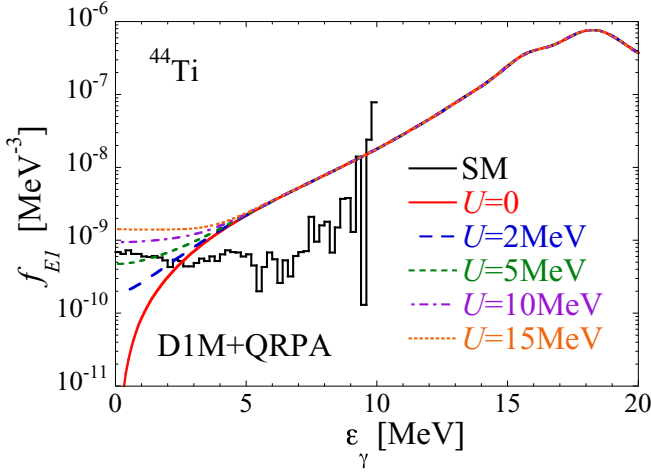


FIG. 5. Illustration for  $^{44}\text{Ti}$  of the low-energy contribution to the  $E1$  strength function [Eq. (1)] applied to the D1M+QRPA strength for various initial excitation energies  $U$ , as suggested by the SM calculations [22]. The values of  $f_0 = 10^{-10} \text{ MeV}^{-4}$  and  $\epsilon_0 = 3 \text{ MeV}$  are used in the empirical low-energy strength.

uncertainties which can be significantly larger and even change the slope of the dipole strength (see Refs. [38,49] for more details).

The present  $E1$  and  $M1$  strengths are also found to be in rather good agreement with the data extracted from average

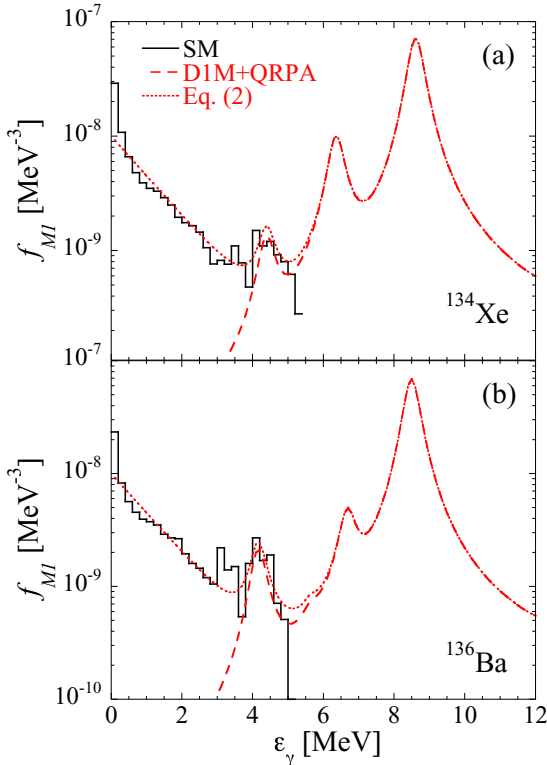


FIG. 6. (a) Illustration for  $^{134}\text{Xe}$  of the low-energy contribution to the  $M1$  strength function [Eq. (2) with  $C = 10^{-8} \text{ MeV}^{-3}$  and  $\eta = 0.8 \text{ MeV}^{-1}$ ] applied to the D1M+QRPA strength, as suggested by the SM calculations. (b) Same for  $^{136}\text{Ba}$ .

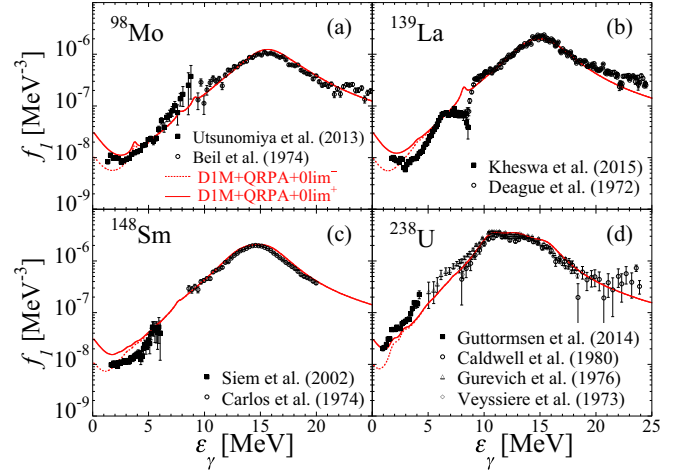


FIG. 7. The D1M + QRPA +  $0\text{lim}^{\pm}$  dipole strength function  $f_{\gamma} = f_{E1} + f_{M1}$  given by Eqs. (1) and (2) compared with experimental photodata and Oslo measurements for (a)  $^{98}\text{Mo}$  [38,39], (b)  $^{139}\text{La}$  [40,41], (c)  $^{148}\text{Sm}$  [42,43], and (d)  $^{238}\text{U}$  [44–47].

resonance capture (ARC) experiments [50]. As shown in Fig. 9, the  $E1$  strength in the 5- to 8-MeV photon energy range where ARC data exist is rather well reproduced by the D1M+QRPA calculation for the 47 nuclei recently reanalyzed. In contrast, the  $M1$  QRPA strength seems to be more systematically underestimated, especially for the spherical  $^{96}\text{Mo}$  and  $^{98}\text{Mo}$  isotopes. For this reason, the  $E1/M1$  ratios are overestimated. Note that the  $E1$  and  $M1$  strengths in the 5–8 MeV photon energy range characterizing the ARC measurements are not affected significantly by the low-energy component [Eqs. (1) and (2)] which becomes relevant only below typically 3–4 MeV.

#### IV. AVERAGE RADIATIVE WIDTH

Among the various experimental data, the average radiative width is known to play a key role in reaction modeling [3]. The average radiative width is defined as [3]

$$\langle \Gamma_{\gamma} \rangle = \frac{D_0}{2\pi} \sum_{X,L,J,\pi} \int_0^{S_n+E_n} T_{XL}(\epsilon_{\gamma}) \times \rho(S_n + E_n - \epsilon_{\gamma}, J, \pi) d\epsilon_{\gamma}, \quad (3)$$

where  $D_0$  is the average resonance spacing for  $s$ -wave neutrons,  $S_n$  is the neutron separation energy,  $E_n$  is the neutron incident energy,

$$T_{XL} = 2\pi \epsilon_{\gamma}^{2L+1} \overleftarrow{f}_{XL}(\epsilon_{\gamma}) \quad (4)$$

is the electromagnetic transmission coefficient ( $X = M$  or  $E$ ) for a multipolarity  $L$ , and  $\rho$  is the energy-, spin- ( $J$ ), and parity- ( $\pi$ ) dependent nuclear level density.

It has been a long-standing problem that phenomenological SLO model [3] tend to overestimate the average radiative width significantly, while its improved and widely used version, the

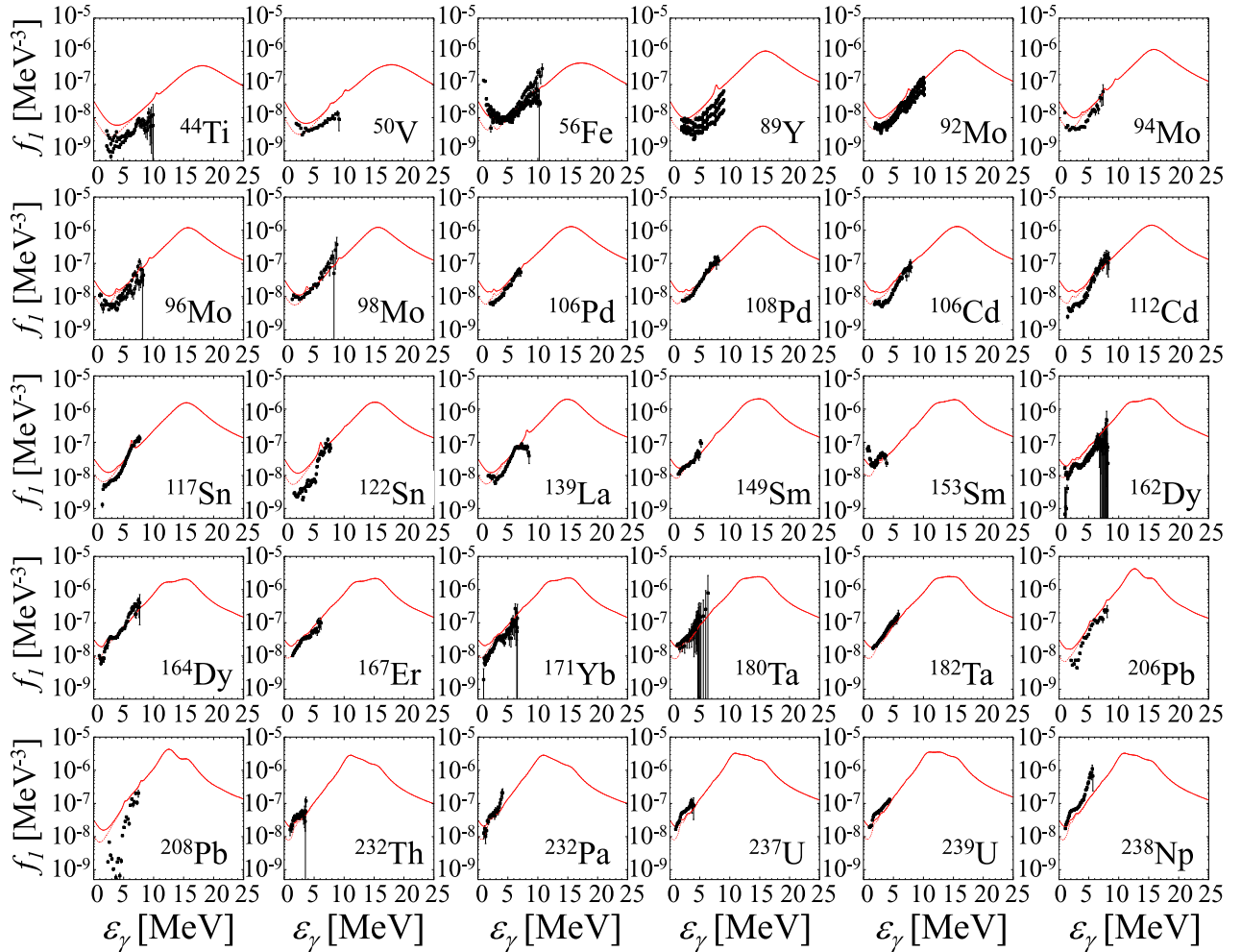


FIG. 8. Comparison of the experimental Oslo strength [48] (black squares) with the DIM + QRPA +  $0\text{lim}^\pm$  predictions (full red lines for  $0\text{lim}^+$  and dotted lines for  $0\text{lim}^-$  parametrization) for 30 nuclei between  $^{44}\text{Ti}$  and  $^{238}\text{Np}$ .

so-called GLO model,<sup>2</sup> underestimates  $\langle\Gamma_\gamma\rangle$ . For this reason, the SLO model also tends to overestimate the radiative neutron capture cross sections for low-energy (keV) neutrons, while the GLO model overestimates them (see also Ref. [51]). Such deviations are shown in Fig. 10 where the experimental average radiative widths are compared with predictions for SLO [3,31], GLO [3,17], and the present DIM + QRPA +  $0\text{lim}^\pm$  [Eqs. (1) and (2)]. It can be seen that, in contrast to the SLO and GLO models, the present DIM + QRPA +  $0\text{lim}^\pm$  strengths (including both the  $M1$  and  $E1$  contributions) reproduce globally rather well the experimental average radiative width. The low-energy components [Eqs. (1) and (2)] contribute in a non-negligible way to the  $\langle\Gamma_\gamma\rangle$  integral [Eq. (3)], especially the  $M1$  upbend for spherical nuclei where a significant additional dipole strength is included at low energies (Fig. 6). Such a

contribution as well as the  $M1$  scissors mode around 3 MeV for deformed nuclei are absent in the Lorentzian approach and explain why the GLO model underestimates the experimental  $\langle\Gamma_\gamma\rangle$ . The average radiative width remains, however, sensitive to the nuclear level densities [see Eq. (3)], as illustrated in Fig. 10 where the error bars on the predictions represent the corresponding sensitivity using different nuclear level density models [52,53].

The deviation with respect to experimental data can be characterized by the root mean square (rms) factors,  $\varepsilon_{\text{rms}}$  and  $f_{\text{rms}}$ , defined as

$$\varepsilon_{\text{rms}} = \exp \left[ \frac{1}{N_e} \sum_{i=1}^{N_e} \ln r_i \right], \quad (5)$$

$$f_{\text{rms}} = \exp \left[ \frac{1}{N_e} \sum_{i=1}^{N_e} \ln^2 r_i \right]^{1/2}, \quad (6)$$

where  $N_e$  is the number of experimental data and  $r_i$  is, for each data point  $i$ , the ratio of theoretical to experimental  $\langle\Gamma_\gamma\rangle$  which takes into account the experimental uncertainties  $\delta_{\text{exp}}$ ,

<sup>2</sup>Note that we will refer here as GLO model the GLO model for the  $E1$  channel supplemented by the SLO model for the  $M1$  component, as defined in the RIPL library [3] and corresponding to the original work of Kopecky *et al.* [17].

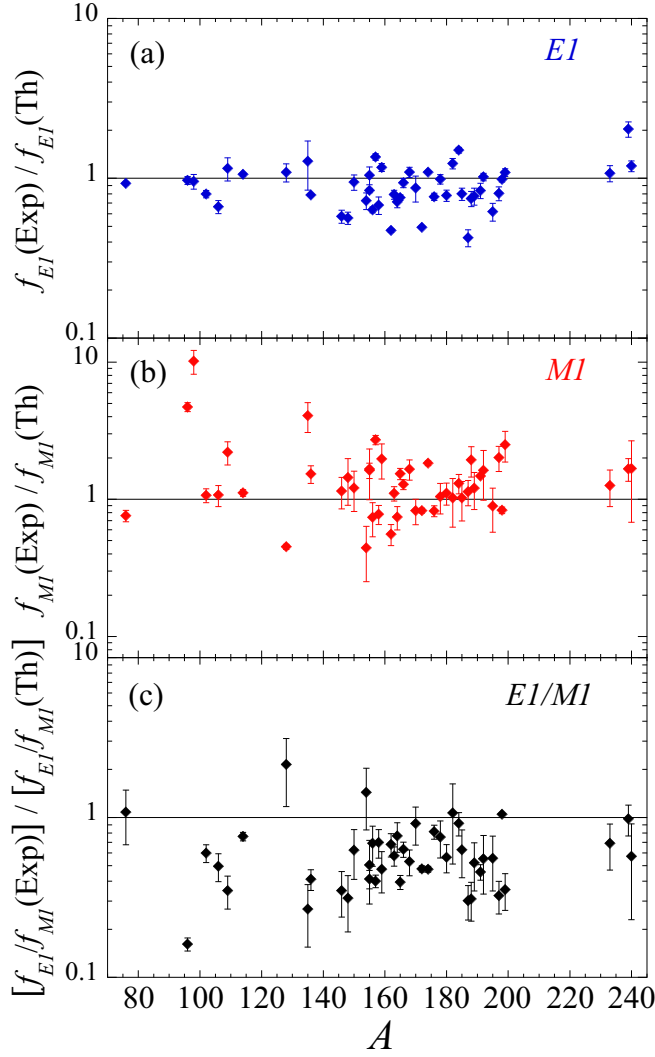


FIG. 9. Comparison between the experimental  $E1$  and  $M1$  strengths from ARC data [50] with the D1M+QRPA+0lim predictions for the 47 nuclei recently reanalyzed. (a)  $E1$  ratios, (b)  $M1$  ratios, and (c)  $E1/M1$  ratios.

more precisely

$$\begin{aligned}
 r &= \frac{\langle \Gamma_\gamma \rangle_{\text{th}}}{\langle \Gamma_\gamma \rangle_{\text{exp}} - \delta_{\text{exp}}} & \text{if } \langle \Gamma_\gamma \rangle_{\text{th}} < \langle \Gamma_\gamma \rangle_{\text{exp}} - \delta_{\text{exp}} \\
 &= \frac{\langle \Gamma_\gamma \rangle_{\text{th}}}{\langle \Gamma_\gamma \rangle_{\text{exp}} + \delta_{\text{exp}}} & \text{if } \langle \Gamma_\gamma \rangle_{\text{th}} > \langle \Gamma_\gamma \rangle_{\text{exp}} + \delta_{\text{exp}} \\
 &= 1 & \text{otherwise.}
 \end{aligned} \quad (7)$$

The closer the  $\varepsilon_{\text{rms}}$  and  $f_{\text{rms}}$  factors are to 1, the better the theory reproduces experimental data within their  $1\text{-}\sigma$  uncertainties. We give in Table I the  $\varepsilon_{\text{rms}}$  and  $f_{\text{rms}}$  factors for the  $\langle \Gamma_\gamma \rangle$  values with respect to the experimental data [3]. While the GLO strength clearly gives large deviations [as seen in Fig. 10(b)], the D1M+QRPA+0lim strength underestimates measured value globally between 12% and 26% for D1M + QRPA + 0lim<sup>-</sup> but is in rather good agreement for the D1M + QRPA + 0lim<sup>+</sup> case, especially with the HFB+Combinatorial

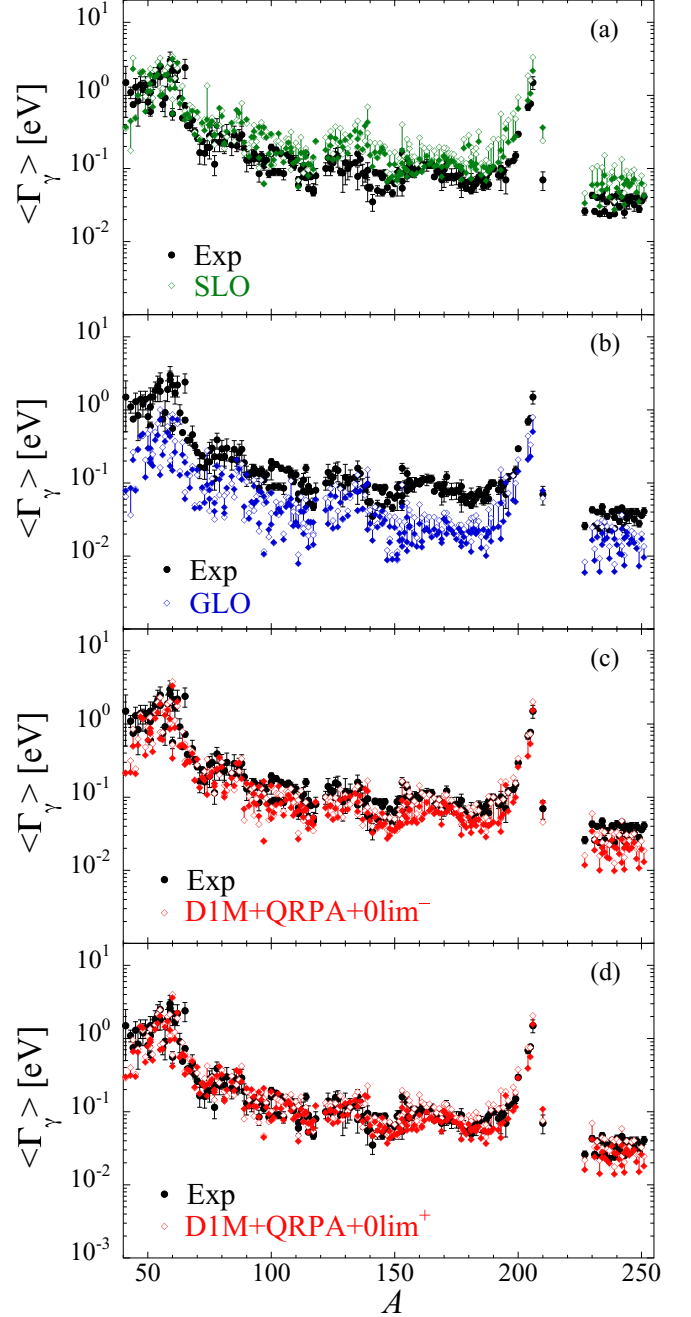


FIG. 10. Comparison between experimental (black circles) [3] and theoretical (colored diamonds) average radiative width  $\langle \Gamma_\gamma \rangle$  as a function of  $A$ . The strength corresponds to (a) the SLO model [3] for both the  $E1$  and  $M1$  strengths, (b) the GLO model [3,17], (c) D1M + QRPA + 0lim<sup>-</sup>, and (d) D1M + QRPA + 0lim<sup>+</sup>. The error bars on the theoretical predictions illustrate the uncertainties associated with the use of different nuclear level density models (open diamonds for the Combinatorial model [52] and full diamonds for the constant temperature model [53]).

level densities. The  $f_{\text{rms}}$  factor in this latter case is as low as 1.27, as confirmed by Fig. 10(d). The constant-temperature level density formula leads systematically to lower predictions of the average radiative width.

TABLE I.  $\varepsilon_{\text{rms}}$  and  $f_{\text{rms}}$  for the theoretical to experimental ratios of both  $\langle\Gamma_\gamma\rangle$  and the MACS  $\langle\sigma\rangle$ . The theoretical estimates are obtained with the present DIM + QRPA +  $0\text{lim}^\pm$  or the Lorentzian (GLO) [3,17] strengths and with either the constant temperature (CT) [53] or the HFB+Combinatorial (Comb) [52] models of nuclear level densities.

	$\langle\Gamma_\gamma\rangle$		$\langle\sigma\rangle$	
	$\varepsilon_{\text{rms}}$	$f_{\text{rms}}$	$\varepsilon_{\text{rms}}$	$f_{\text{rms}}$
$0\text{lim}^-$ (Comb)	0.88	1.35	1.07	1.44
$0\text{lim}^-$ (CT)	0.74	1.55	0.95	1.37
$0\text{lim}^+$ (Comb)	1.02	1.27	1.30	1.55
$0\text{lim}^+$ (CT)	0.90	1.32	1.15	1.40
GLO (Comb)	0.48	2.44	0.61	1.92
GLO (CT)	0.38	3.02	0.53	2.07

## V. RADIATIVE NUCLEON CAPTURES

The radiative neutron and proton capture cross sections and reaction rates of astrophysical interest have been calculated systematically on the basis of the Hauser-Feshbach statistical model described by the TALYS reaction code [54]. The widely used GLO model [3,17] is considered here for a comparison with the present DIM+QRPA+ $0\text{lim}$  model. Either the HFB plus combinatorial model of nuclear level densities [52] or the constant temperature plus Fermi gas model [53] are adopted for the cross-section calculations. When no experimental masses [55] are available, the HFB-31 mass model is used [56].

Figure 11 illustrates the impact of the low-energy  $M1$  strength on the radiative neutron capture cross section. The low-energy  $E1$  component [Eq. (1)] has a rather negligible

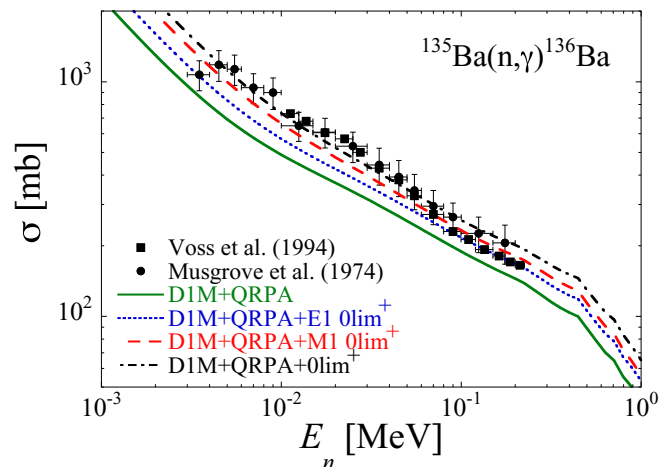


FIG. 11.  $^{135}\text{Ba}(n, \gamma)^{136}\text{Ba}$  cross section, as a function of the neutron energy, obtained with the DIM+QRPA  $E1$  and  $M1$  strengths (solid line). The dotted, dashed, and dash-dot lines show the impact of the low-energy  $E1$  limit [Eq. (1)], the  $M1$  limit [Eq. (2)], or both, respectively. The  $0\text{lim}^+$  parametrization of the zero limit is used as well as the combinatorial nuclear level density model [52]. The experimental data are taken from Refs. [57,58].

effect; it increases the cross section by no more than 20% in the  $0\text{lim}^+$  case (and only 2% in the  $0\text{lim}^-$  case) due to the  $\varepsilon_\gamma^3$  dependence weighting the  $\gamma$ -ray strength function in the calculation of the transmission coefficient  $T_{E1}$  [see Eq. (4)]. The  $M1$  upbend is seen to increase the cross section by about 40% in the  $0\text{lim}^+$  case (though only 10% in the  $0\text{lim}^-$  case), although the  $M1$  low-energy contribution is located below 4 MeV (Fig. 6). The exponential increase of the  $M1$  strength at decreasing energies [Eq. (2)] counterbalances the  $\varepsilon_\gamma^3$  effect in the calculation of  $T_{M1}$  [Eq. (4)] and leads to the non-negligible impact on the cross section. The inclusion of both the  $E1$  and  $M1$  low-energy limits is also seen to give a cross section reproducing experimental data significantly better than without such contributions (Fig. 11).

Figure 12 compares the 240 experimental neutron Maxwellian-averaged capture cross sections (MACS) [59] at 30 keV (assuming the target in its ground state only) for nuclei with  $20 \leq Z \leq 83$  with the TALYS predictions obtained either with the GLO model or the DIM + QRPA +  $0\text{lim}^-$  model. Both the HFB+Combinatorial and constant temperature models of nuclear level densities are considered. Note that in the TALYS calculation the strength function is not renormalized to reproduce the experimental average radiative width. Only nuclei with  $Z \geq 20$  are considered in the comparison to ensure the validity of the Hauser-Feshbach approach, the cross section for lighter nuclei being affected by the direct contribution [2] and the resolved resonance regime [60] at the 30-keV neutron energies considered here. The deviation with respect to experimental data can be characterized by the same  $\varepsilon_{\text{rms}}$  and  $f_{\text{rms}}$  factors as defined for the average radiative width [Eqs. (5) and (6)]. In this case, the experimental error bars are usually rather small (a few percentages), so that  $r_i = \langle\sigma\rangle_{\text{th}}^i / \langle\sigma\rangle_{\text{exp}}^i$  and the uncertainties have a small impact on the calculation of the rms factors. As shown in Table I, the rms deviation factors are better reproduced with DIM + QRPA +  $0\text{lim}^-$  parametrization and optimum when using the constant temperature formula for level densities. The DIM + QRPA +  $0\text{lim}^+$  that used to optimize the experimental average radiative widths slightly overestimate the MACS.

In the GLO case, a  $f_{\text{rms}}$  deviation of about 2 and mean deviation  $\varepsilon_{\text{rms}}$  significantly lower than 1 are obtained on the theoretical to experimental MACS ratios (Table I). The MACS like the average radiative widths are clearly underestimated [compare Figs. 10(b) and 12(a)]. This explains why reaction codes need to renormalize the  $E1$  strength function on experimental average radiative width to reproduce accurately the radiative neutron capture cross section. However, such a renormalization, if efficient at low neutron energies to compensate the missing strength, may lead to different energy dependencies of the neutron capture cross section. An example is provided for  $^{101}\text{Mo}$  in Fig. 13 where the GLO strength gives  $\langle\Gamma_\gamma\rangle_{\text{GLO}} = 0.15$  eV, i.e., a factor of 6 lower than then experimental value  $\langle\Gamma_\gamma\rangle_{\text{exp}} = 0.09 \pm 0.01$  eV [3]. As seen in Fig. 13(b), such a low dipole strength leads to a neutron capture cross section a factor of about 4–5 lower than experimental data. Multiplying artificially the overall  $E1$  strength by a factor  $g_{\text{norm}} = \langle\Gamma_\gamma\rangle_{\text{exp}} / \langle\Gamma_\gamma\rangle_{\text{GLO}} = 6$  provides, however, a cross section in good agreement at low energies



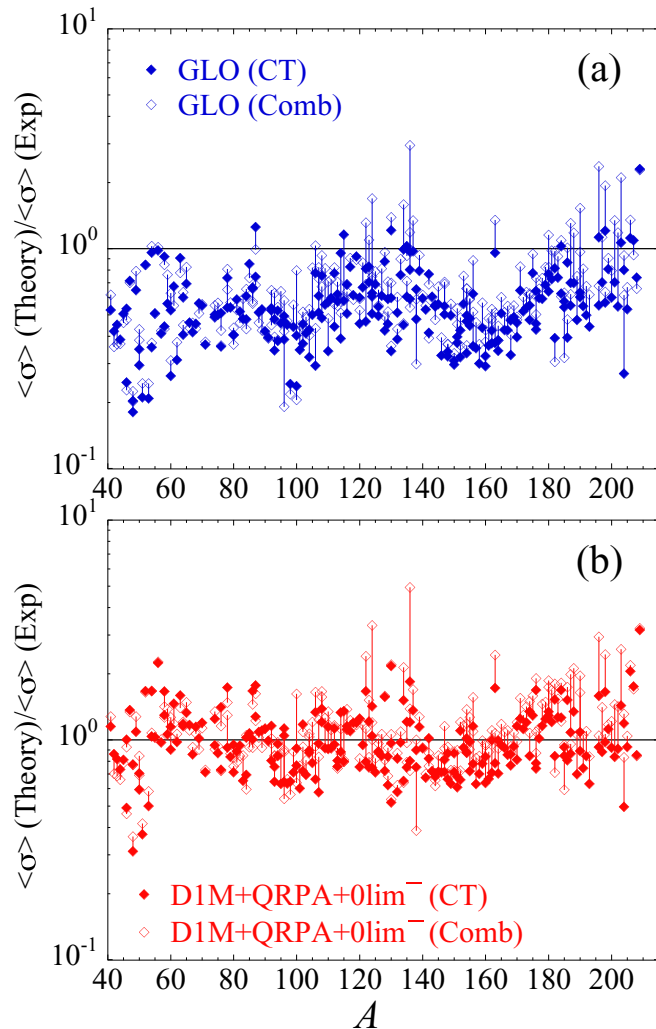


FIG. 12. Ratio of the theoretical to experimental MACS at  $kT = 30$  keV as a function of the atomic mass  $A$  for all nuclei between Ca and Bi for which experimental MACS exist [59]. (a) The theoretical MACS are obtained with the GLO model [3,17]. (b) Same as in (a) when the MACS are obtained with the present D1M + QRPA + 0lim<sup>-</sup>. In both panels, the full symbols are calculations with the HFB+Combinatorial model of nuclear level densities [52] and the open symbols with the constant temperature plus Fermi gas model [53].

with experimental data. Such a renormalization has become a default procedure in most of the reaction codes. In contrast, the D1M + QRPA + 0lim<sup>+</sup> strength gives an average radiative width of 0.082 eV in agreement with experiments and therefore does not need to be renormalized. It is seen in Fig. 13(a) to be relatively close to the renormalized GLO strength at low energies, hence giving rise to relatively similar cross section for keV neutrons. However, at neutron energies above 1 MeV, significant deviations between the cross sections obtained with the renormalized GLO and D1M+QRPA+0lim strengths can be observed since both strengths differ now in the energy region of relevance, i.e., in the GDR region. The long-standing problem between the compatibility of the predicted radiative width and experimental capture and photo data is largely solved

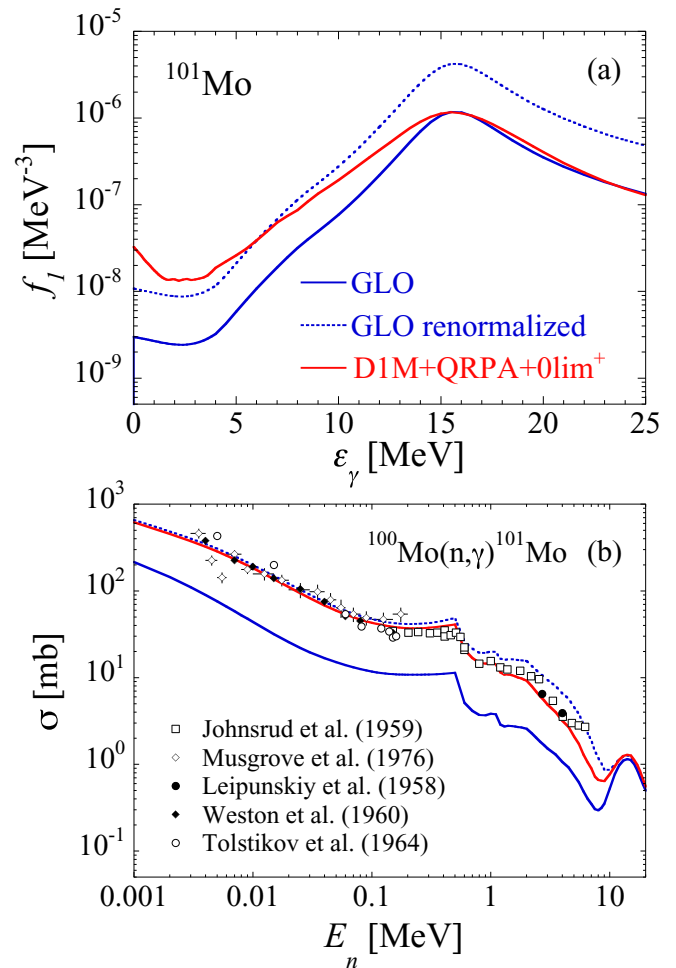


FIG. 13. (a)  $E1 + M1$  dipole strength of  $^{101}\text{Mo}$  calculated with the GLO model [3] (solid blue line), with the GLO after renormalizing the  $E1$  strength by a factor of 6 (dotted line) and with D1M + QRPA + 0lim<sup>+</sup> (solid red line). (b)  $^{100}\text{Mo}(n, \gamma)^{101}\text{Mo}$  cross sections calculated with the GLO (solid blue line), renormalized GLO (dotted line), and D1M + QRPA + 0lim<sup>+</sup> (red solid line) dipole strength functions. Also shown are the experimental data from Refs. [61–65].

with the present D1M+QRPA+0lim model where both the average radiative width and neutron capture cross sections are consistently estimated and globally in agreement with experimental data, including photoabsorption and photodeexcitation data, as discussed in Secs. II and III. Such a conclusion holds regardless of the nuclear level density model adopted.

Figures 14 and 15 show the ratio of the MACS at a temperature  $T = 10^9$  K typical of the  $r$ -process nucleosynthesis [1] obtained with the present D1M + QRPA + 0lim<sup>+</sup> to those obtained with the GLO model recommended in Refs. [3,17]. When approaching the neutron dripline ( $S_n = 0$ ), the MACS calculated with D1M+QRPA+0lim strength is seen to be a factor up to 500 larger than the one obtained with the traditional GLO model. The most significant effects responsible for such an increase of the MACS are (i) the low-energy  $E1$  strength predicted for neutron-rich nuclei by the D1M+QRPA approach (as already discussed in Ref. [7]) and (ii) the low-energy  $M1$  upbend introduced in Eq. (2). In particular, the

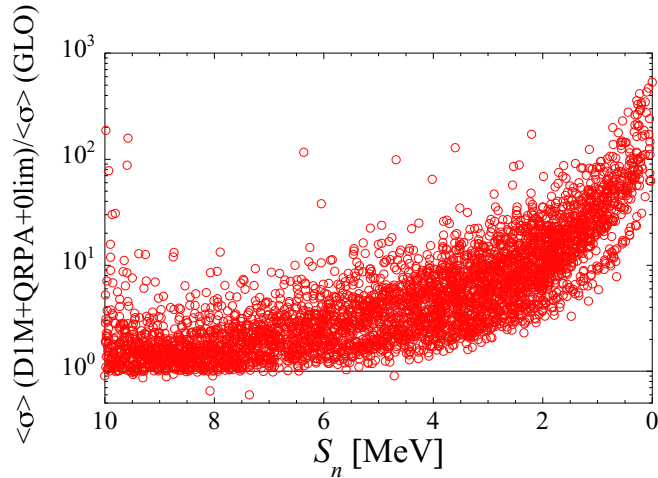


FIG. 14. Ratio of the  $(n, \gamma)$  MACS at  $T = 10^9$  K obtained with the present DIM + QRPA +  $0\text{lim}^+$  [Eqs. (1) and (2)] to the one obtained with the GLO model [3,17]. The ratio is given for all nuclei with  $8 \leq Z \leq 94$  lying between the proton and neutron driplines as a function of the neutron separation energy  $S_n$ . The HFB plus combinatorial model of nuclear level densities is adopted [52].

$M1$  upbend can affect the MACS of exotic neutron-rich nuclei by a factor up to 100. In contrast, the low-energy limit of the  $E1$  strength function included in Eq. (1) only affects the MACS by 20 to 50% due to the  $\varepsilon_\gamma^3$  dependence weighting the  $\gamma$ -ray strength function, as discussed in Sec. IV. This is not the case for the  $M1$  upbend, where the fast increase of the  $M1$  strength at decreasing energies approaching zero is capable of counterbalancing the  $\varepsilon_\gamma^3$  effect in the calculation of  $T_{M1}$ , as also shown in Fig. 11. This effect becomes dominant for exotic neutron-rich region with low neutron separation energy ( $S_n \lesssim 2$  MeV). As far as the HFB+QRPA prediction of the  $M1$  spin flip is concerned, it is almost always insignificant with respect to the stronger  $E1$  contribution at the relevant energies of 8–9 MeV, so that its impact on the MACS is reduced to no more than 10% in comparison with the MACS obtained with

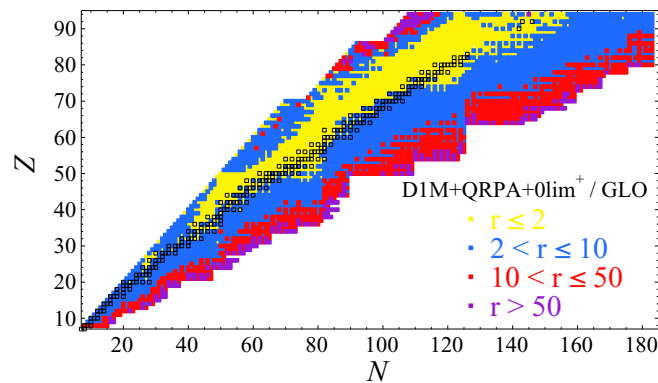


FIG. 15. Color-coded representation in the  $(N, Z)$  plane of the ratio of the  $(n, \gamma)$  MACS at  $T = 10^9$  K obtained with the present DIM + QRPA +  $0\text{lim}^+$  [Eqs. (1) and (2)] to the one obtained with the GLO model [3,17]. Open black squares correspond to the stable nuclei and very long-lived actinides.

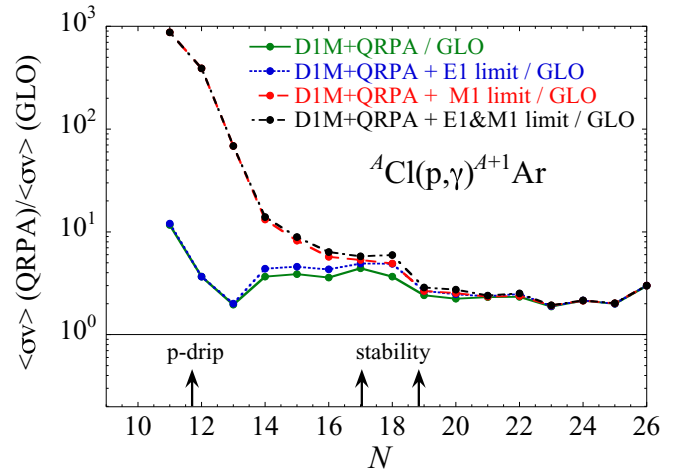


FIG. 16. Ratio of the Maxwellian-averaged astrophysical  $\text{Cl}(p, \gamma)$  reaction rates  $\langle\sigma v\rangle$  at  $T = 2 \times 10^9$  K obtained with the present DIM + QRPA +  $0\text{lim}^+$  to the one obtained with the GLO model [3,17] for the Cl isotopes. The dotted, dashed, and dash-dot lines show the impact on the  $p$ -capture rates of the low-energy  $E1$  limit [Eq. (1)], the  $M1$  limit [Eq. (2)], or both, respectively. The proton drip line is indicated at  $N = 12$  and the valley of  $\beta$  stability at  $N = 18$  and  $N = 20$ .

the SLO  $M1$  strength [3]. Finally, the low-energy  $M1$  scissors mode predicted in deformed nuclei by the HFB+QRPA can impact the MACS by a factor of 2. This extra strength is never included in cross-section calculations based on the Lorentzian-type strength functions, except recently through a phenomenological approximation [51]. It affects the average radiative width as well as the neutron capture cross section of deformed nuclei in a non-negligible way.

In comparison with the traditional GLO approach, the HFB+QRPA strength function affects not only the radiative neutron capture cross section but also the radiative proton capture cross section on the neutron-deficient side of the valley of  $\beta$  stability. For such neutron-deficient nuclei, the QRPA calculation predicts extra  $E1$  strength at energies around a few MeV, leading to an increase of the electromagnetic deexcitation transmission coefficient in the compound nucleus. As shown in Fig. 16, the proton capture by Cl neutron-deficient isotopes is a few times larger with the DIM+QRPA strength in comparison with GLO. While the low-energy  $E1$  contribution may affect the reaction rate by a factor of 2, the low-energy  $M1$  upbend added to the DIM+QRPA strength [Eq. (2)] is seen to have an even larger impact on the radiative proton capture rate for the most exotic neutron-deficient Cl isotopes with an increase of the rate by a factor 800 in the case of  ${}^{29}\text{Cl}(p, \gamma) {}^{30}\text{Ar}$ . In Fig. 17, the proton MACS at a temperature typical of the  $p$ -processes nucleosynthesis [66] of  $T = 2 \times 10^9$  K is compared systematically, for all nuclei with  $8 \leq Z \leq 94$  lying between the proton and neutron drip lines, when use is made of the Lorentzian-type or the QRPA approaches. The proton MACS of light  $n$ -deficient nuclei up to Sn appears to be significantly affected by a factor as high as a few hundreds. Interestingly, deformed stable or slightly neutron-rich nuclei with  $60 \lesssim Z \lesssim 80$  and in the actinide region also present an

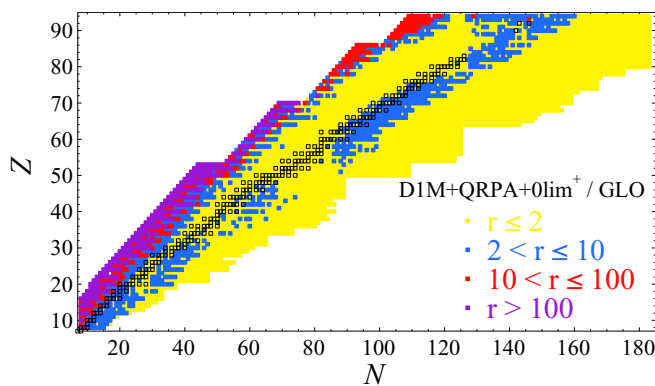


FIG. 17. Color-coded representation in the  $(N, Z)$  plane of the ratio of the  $(p, \gamma)$  MACS at  $T = 2 \times 10^9$  K obtained with the present DIM + QRPA +  $0\text{lim}^+$  [Eqs. (1) and (2)] to the one obtained with the GLO model [3,17]. Open black squares correspond to the stable and very long-lived nuclei.

increase of their proton MACS by a factor 2–3, essentially due to the larger  $E1$  strength in the low-energy tail of the GDR with respect to the GLO approach (see also Ref. [7]).

## VI. CONCLUSIONS

HFB+QRPA models are now available for applications and have shown their capacity to predict photoabsorption  $\gamma$ -ray strength functions. Effects beyond the one-particle–one-hole excitations and the interaction between the single-particle and low-lying collective phonon degrees of freedom can be empirically taken into account by renormalizing the HFB+QRPA strength through an energy shift and a damping width. A simple prescription has been proposed and shown to reproduce the GDR properties fairly well. It also agrees satisfactorily with newly derived ARC data though it seems to underestimated

slightly the  $M1$  channel. The axially symmetric deformed QRPA calculation also allows us to estimate coherently the contribution of the scissors mode.

We have extended our HFB+QRPA calculations of the photoabsorption strength to the determination of the deexcitation strength function. To do so, SM calculations of the deexcitation dipole strength function as well as experimental data have been considered to provide insight in the low-energy limit. Those suggest that at photon energies approaching the zero limit, the  $E1$  strength remains constant while the  $M1$  strength increases exponentially. We showed that, in a first approximation, the HFB+QRPA strength can be complemented by simple analytical expressions to account for the missing strength at the lowest energies approaching zero. These contributions have been shown to reproduce satisfactorily experimental data at low energies but also to affect significantly the calculation of the average radiative width as well as radiative nucleon capture cross sections. Although the additional dipole strength is located at low energies, typically below 3–4 MeV, it impacts the overall radiative width, especially due to the increasing  $M1$  strength at decreasing photon energies. This extra strength can affect the radiative neutron capture cross section of neutron-rich nuclei as well as proton capture cross section of neutron-deficient nuclei by factors up to a few hundreds for the most exotic nuclei. Future work will need to estimate such low-energy contribution to the dipole strength more systematically and on the basis of microscopic models, including continuum temperature-dependent QRPA and beyond QRPA calculations.

## ACKNOWLEDGMENTS

S.G. acknowledges the support of the FRS-FNRS. This work was performed within the IAEA CRP on “Updating the Photonuclear data Library and generating a Reference Database for Photon Strength Functions” (F410 32). The authors also thank J. Kopecky for providing updated ARC data.

- 
- [1] M. Arnould, S. Goriely, and K. Takahashi, *Phys. Rep.* **450**, 97 (2007).
- [2] Y. Xu, S. Goriely, A. J. Koning, and S. Hilaire, *Phys. Rev. C* **90**, 024604 (2014).
- [3] R. Capote, M. Herman, P. Oblozinsky, P. Young, S. Goriely, T. Belgya, A. Ignatyuk, A. Koning, S. Hilaire, V. Plujko, M. Avrigeanu, O. Bersillon *et al.*, *Nucl. Data Sheets* **110**, 3107 (2009).
- [4] S. Goriely and E. Khan, *Nucl. Phys. A* **706**, 217 (2002).
- [5] S. Goriely, E. Khan, and M. Samyn, *Nucl. Phys. A* **739**, 331 (2004).
- [6] I. Daoutidis and S. Goriely, *Phys. Rev. C* **86**, 034328 (2012).
- [7] M. Martini, S. Péru, S. Hilaire, S. Goriely, and F. Lechaftois, *Phys. Rev. C* **94**, 014304 (2016).
- [8] S. Goriely, S. Hilaire, S. Péru, M. Martini, I. Deloncle, and F. Lechaftois, *Phys. Rev. C* **94**, 044306 (2016).
- [9] G. Colò and P. Bortignon, *Nucl. Phys. A* **696**, 427 (2001).
- [10] D. Sarchi, P. Bortignon, and G. Colò, *Phys. Lett. B* **601**, 27 (2004).
- [11] N. Tsoneva and H. Lenske, *Phys. Rev. C* **77**, 024321 (2008).
- [12] P. Papakonstantinou and R. Roth, *Phys. Lett. B* **671**, 356 (2009).
- [13] O. Achakovskiy, A. Avdeenkov, S. Goriely, S. Kamedzhiev, and S. Krewald, *Phys. Rev. C* **91**, 034620 (2015).
- [14] D. Gambacurta, M. Grasso, and O. Vasseur, *Phys. Lett. B* **777**, 163 (2018).
- [15] E. Litvinova, P. Ring, and V. Tselyaev, *Phys. Rev. C* **88**, 044320 (2013).
- [16] I. A. Egorova and E. Litvinova, *Phys. Rev. C* **94**, 034322 (2016).
- [17] J. Kopecky and M. Uhl, *Phys. Rev. C* **41**, 1941 (1990).
- [18] A. Voinov, E. Algin, U. Agvaanluvsan, T. Belgya, R. Chankova, M. Guttormsen, G. E. Mitchell, J. Rekstad, A. Schiller, and S. Siem, *Phys. Rev. Lett.* **93**, 142504 (2004).
- [19] M. Guttormsen, R. Chankova, U. Agvaanluvsan, E. Algin, L. A. Bernstein, F. Ingelbretsen, T. Lönnroth, S. Messelt, G. E. Mitchell, J. Rekstad, A. Schiller, S. Siem *et al.*, *Phys. Rev. C* **71**, 044307 (2005).
- [20] R. Schwengner, S. Frauendorf, and A. C. Larsen, *Phys. Rev. Lett.* **111**, 232504 (2013).
- [21] B. A. Brown and A. C. Larsen, *Phys. Rev. Lett.* **113**, 252502 (2014).
- [22] K. Sieja, *Phys. Rev. Lett.* **119**, 052502 (2017).

- [23] K. Sieja, *Europhys. J. Web Conf.* **146**, 05004 (2017).
- [24] S. Karampagia, B. A. Brown, and V. Zelevinsky, *Phys. Rev. C* **95**, 024322 (2017).
- [25] R. Schwengner, S. Frauendorf, and B. A. Brown, *Phys. Rev. Lett.* **118**, 092502 (2017).
- [26] S. Péru and H. Goutte, *Phys. Rev. C* **77**, 044313 (2008).
- [27] S. Péru, G. Gosselin, M. Martini, M. Dupuis, S. Hilaire, and J.-C. Devaux, *Phys. Rev. C* **83**, 014314 (2011).
- [28] S. Péru and M. Martini, *Eur. Phys. J. A* **50**, 88 (2014).
- [29] I. Deloncle, S. Péru, and M. Martini, *Eur. Phys. J. A* **53**, 170 (2017).
- [30] S. Goriely, S. Hilaire, M. Girod, and S. Péru, *Phys. Rev. Lett.* **102**, 242501 (2009).
- [31] V. Plujko, R. Capote, and O. Gorbachenko, *At. Data Nucl. Data Tables* **97**, 567 (2011).
- [32] S. Hilaire, M. Girod, S. Goriely, and A. J. Koning, *Phys. Rev. C* **86**, 064317 (2012).
- [33] EXFOR, *Experimental Nuclear Reaction Data* (2017) [<https://www-nds.iaea.org/exfor>].
- [34] P. Ring, L. Robledo, J. Egido, and M. Faber, *Nucl. Phys. A* **419**, 261 (1984).
- [35] E. Litvinova and N. Belov, *Phys. Rev. C* **88**, 031302(R) (2013).
- [36] E. Yüksel, G. Colò, E. Khan, Y. F. Niu, and K. Bozkurt, *Phys. Rev. C* **96**, 024303 (2017).
- [37] E. Algin, U. Agvaanluvsan, M. Guttormsen, A. C. Larsen, G. E. Mitchell, J. Rektstad, A. Schiller, S. Siem, and A. Voinov, *Phys. Rev. C* **78**, 054321 (2008).
- [38] H. Utsunomiya, S. Goriely, T. Kondo, C. Iwamoto, H. Akimune, T. Yamagata, H. Toyokawa, H. Harada, F. Kitatani, Y.-W. Lui, A. Larsen, M. Guttormsen *et al.*, *Phys. Rev. C* **88**, 015805 (2013).
- [39] H. Beil, R. Bergere, P. Carlos, A. Lepretre, A. D. Miniac, and A. Veyssière, *Nucl. Phys. A* **227**, 427 (1974).
- [40] T. Deague and R. Stewart, *Nucl. Phys. A* **191**, 305 (1972).
- [41] B. Kheswa, M. Wiedeking, F. Giacoppo, S. Goriely, M. Guttormsen, A.-C. Larsen, F. Bello Garrote, T. Eriksen, A. Görge, T. Hagen, P. Koehler, M. Klintefjord *et al.*, *Phys. Lett. B* **744**, 268 (2015).
- [42] S. Siem, M. Guttormsen, K. Ingeberg, E. Melby, J. Rektstad, A. Schiller, and A. Voinov, *Phys. Rev. C* **65**, 044318 (2002).
- [43] P. Carlos, H. Beil, R. Bergere, A. Lepretre, A. D. Miniac, and A. Veyssière, *Nucl. Phys. A* **225**, 171 (1974).
- [44] M. Guttormsen, L. A. Bernstein, A. Görge, B. Jurado, S. Siem, M. Aiche, Q. Ducasse, F. Giacoppo, F. Gunsing, T. W. Hagen, A. C. Larsen, M. Lebois *et al.*, *Phys. Rev. C* **89**, 014302 (2014).
- [45] J. T. Caldwell, E. J. Dowdy, B. L. Berman, R. A. Alvarez, and P. Meyer, *Phys. Rev. C* **21**, 1215 (1980).
- [46] G. Gurevich, L. Lazareva, V. Mazur, G. Solodukhov, and B. Tulupov, *Nucl. Phys. A* **273**, 326 (1976).
- [47] A. Veyssière, H. Beil, R. Bergère, P. Carlos, A. Lepretre, and K. Kernbath, *Nucl. Phys. A* **199**, 45 (1973).
- [48] Oslo database, Level densities and gamma-ray strength functions (2017) [<http://www.mn.uio.no/fysikk/english/research/about/infrastructure/OCL/nuclear-physics-research/compilation/>].
- [49] B. V. Kheswa, M. Wiedeking, J. A. Brown, A. C. Larsen, S. Goriely, M. Guttormsen, F. L. B. Garrote, L. A. Bernstein, D. L. Bleuel, T. K. Eriksen, F. Giacoppo, A. Gorgen *et al.*, *Phys. Rev. C* **95**, 045805 (2017).
- [50] J. Kopecky, S. Goriely, S. Péru, S. Hilaire, and M. Martini, *Phys. Rev. C* **95**, 054317 (2017).
- [51] M. R. Mumpower, T. Kawano, J. L. Ullmann, M. Krčička, and T. M. Sprouse, *Phys. Rev. C* **96**, 024612 (2017).
- [52] S. Goriely, S. Hilaire, and A. J. Koning, *Phys. Rev. C* **78**, 064307 (2008).
- [53] A. Koning, S. Hilaire, and S. Goriely, *Nucl. Phys. A* **810**, 13 (2008).
- [54] A. Koning and D. Rochman, *Nucl. Data Sheets* **113**, 2841 (2012) [<http://www.sciencedirect.com/science/article/pii/S0090375212000889>].
- [55] M. Wang, G. Audi, F. Kondev, W. Huang, S. Naimi, and X. Xu, *Chin. Phys. C* **41** (4), 030003 (2017).
- [56] S. Goriely, N. Chamel, and J. M. Pearson, *Phys. Rev. C* **93**, 034337 (2016).
- [57] F. Voss, K. Wisshak, K. Guber, F. Käppeler, and G. Reffo, *Phys. Rev. C* **50**, 2582 (1994).
- [58] A. D. Musgrove, B. Allen, and R. Macklin, *Austr. AEC Rep.* **327**, 1 (1974).
- [59] I. Dillmann, M. Heil, F. Käppeler, R. Plag, T. Rauscher, and F.-K. Thielemann, *AIP Conf. Proc.* **819**, 123 (2006).
- [60] D. Rochman, S. Goriely, A. Koning, and H. Ferroukhi, *Phys. Lett. B* **764**, 109 (2017).
- [61] A. Johnsrud, M. Silbert, and H. Barschall, *Phys. Rev.* **116**, 927 (1959).
- [62] A. D. Musgrove, B. Allen, J. W. Boldeman, and R. L. Macklin, *Nucl. Phys. A* **270**, 108 (1976).
- [63] A. Leipunskiy, O. Kazachkovskiy, G. Artyukhov, A. I. Baryshnikov, T. Belanova, V. Galkov, Y. Stavisskiy, E. Stumbur, and L. Sherman, *Sec. Int. At. En. Conf.* **15**, 50 (1958).
- [64] L. Weston, K. Seth, E. Bilpuch, and H. Newson, *Ann. Phys.* **10**, 477 (1960).
- [65] V. Tolstikov, V. Kolesov, A. Dovbenko, and J. Stavisskiy, *Atom. Energ.* **17**, 505 (1964).
- [66] M. Arnould and S. Goriely, *Phys. Rep.* **384**, 1 (2003).